Baryon-induced Collapse of Dark Matter Cores into Supermassive Black Holes

C. R. Argüelles[1,2] , J. A. Rueda[2,3,4,5,6] , and R. Ruffini[2,4,7,8]

[1] Instituto de Astrofísica de La Plata, UNLP-CONICET, Paseo del Bosque s/n B1900FWA La Plata, Argentina
[2] ICRANet, Piazza della Repubblica 10, I-65122 Pescara, Italy; carguelles@fcaglp.unlp.edu.ar, jorge.rueda@icra.it, ruffini@icra.it
[3] ICRANet-Ferrara, Dip. di Fisica e Scienze della Terra, Università degli Studi di Ferrara, Via Saragat 1, I-44122 Ferrara, Italy
[4] ICRA, Dipartamento di Fisica, Sapienza Università di Roma, Piazzale Aldo Moro 5, I-00185 Rome, Italy
[5] Department of Physics and Earth Science, University of Ferrara, Via Saragat 1, I-44122 Ferrara, Italy
[6] INAF, Istituto di Astrofisica e Planetologia Spaziali, Via Fosso del Cavaliere 100, I-00133 Rome, Italy
[7] Université de Nice Sophia-Antipolis, Grand Château Parc Valrose, Nice, CEDEX 2, France
[8] INAF, Viale del Parco Mellini 84, I-00136 Rome, Italy

Abstract

Nonlinear structure formation for fermionic dark matter particles leads to dark matter density profiles with a degenerate compact core surrounded by a diluted halo. For a given fermion mass, the core has a critical mass that collapses into a supermassive black hole (SMBH). Galactic dynamics constraints suggest a $\sim 100\,\mathrm{keV}/c^2$ fermion, which leads to $\sim 10^7 M_\odot$ critical core mass. Here, we show that baryonic (ordinary) matter accretion drives an initially stable dark matter core to SMBH formation and determines the accreted mass threshold that induces it. Baryonic gas density ρ_b and velocity v_b inferred from cosmological hydrosimulations and observations produce sub-Eddington accretion rates triggering the baryon-induced collapse in less than 1 Gyr. This process produces active galactic nuclei in galaxy mergers and the high-redshift Universe. For TXS 2116–077, merging with a nearby galaxy, the observed $3 \times 10^7 M_\odot$ SMBH, for $Q_b = \rho_b/v_b^3 = 0.125 M_\odot/(100\,\mathrm{km\,s^{-1}\,pc})^3$, forms in ≈ 0.6 Gyr, consistent with the 0.5–2 Gyr merger timescale and younger jet. For the farthest central SMBH detected by the Chandra X-ray satellite in the $z = 10.3$ UHZ1 galaxy observed by the James Webb Space Telescope (JWST), the mechanism leads to a $4 \times 10^7 M_\odot$ SMBH in 87–187 Myr, starting the accretion at $z = 12$–15. The baryon-induced collapse can also explain the $\approx 10^7$–$10^8 M_\odot$ SMBHs revealed by JWST at $z \approx 4$–6. After its formation, the SMBH can grow to a few $10^9 M_\odot$ in timescales shorter than 1 Gyr via sub-Eddington baryonic mass accretion.

Unified Astronomy Thesaurus concepts: High-redshift galaxies (734); Active galactic nuclei (16); Supermassive black holes (1663); Galaxy dark matter halos (1880); Dark matter (353); Gravitational collapse (662)

1. Introduction

The standing problem of early formation and growth of supermassive black holes (SMBHs) poses a significant challenge to our current cosmological understanding. Directly related open issues include which is the main channel for the formation of the SMBH seeds in the high-z Universe and how such a black hole (BH)-seed mass correlates with the hosting halo mass in the given cosmological evolution (see, e.g., Inayoshi et al. 2020; Volonteri et al. 2021; Arita et al. 2023; Bogdan et al. 2023a; Larson et al. 2023; Pacucci et al. 2023, and references therein). Standard baryonic channels are based on the growth of BH seeds of $\lesssim 10^2 M_\odot$ from the collapse of Population III stars (Madau & Rees 2001; Hosokawa et al. 2016) or of 10^4–$10^5 M_\odot$ from the direct collapse of gaseous configurations in a plethora of physical setups (Begelman et al. 2006, 2008; Woods et al. 2017; Latif et al. 2022; Zhu et al. 2022). These models are in tension with observations since the BH seeds of 10^2–$10^5 M_\odot$ cannot grow to $\sim 10^9 M_\odot$ sufficiently fast to explain observations at high redshift, e.g., $z \sim 6$ unless ad hoc or extreme assumptions are made (e.g., sustained Eddington or super-Eddington accretion rates for long cosmological times; Yang et al. 2021) limiting the generality of hydrodynamic numerical simulations (see, e.g., Zhu et al. 2022). Such tension is increasing with the daily James Webb

Space Telescope (JWST) observations and new data of quasars at high redshift (e.g., $z \sim 6$–7; Yang et al. 2021; Yue et al. 2023), exploring the faint end of the SMBH luminosity function, unveiling a larger population than previously thought (see Gilli et al. 2022; Kocevski et al. 2023; Maiolino et al. 2023; Fan et al. 2023 for a recent review).

Recently, a new SMBH formation channel has been proposed based on the gravitational collapse of dark matter cores of $\sim 10^7 M_\odot$, made of $\sim 100\,\mathrm{keV}/c^2$ fermions (Argüelles et al. 2023b). The cores are those of the dense core-diluted halo dark matter galactic profiles predicted by the Ruffini–Argüelles–Rueda (RAR) model (Ruffini et al. 2015; Argüelles et al. 2018; see the next section for details). These core–halo density profiles explain a variety of galactic observables, including the flat rotation curves (Argüelles et al. 2018; Krut et al. 2023), galactic universal relations (Argüelles et al. 2019; Krut et al. 2023), and the motion of the innermost stars near the Milky Way's center (Becerra-Vergara et al. 2020, 2021; Argüelles et al. 2022). Argüelles et al. (2023b) showed that starting from the BH seeds produced by the collapse of these dark matter cores, SMBHs of a few $10^9 M_\odot$ can form in less than 1 Gyr by accreting baryonic matter at sub-Eddington rates.

The appeal of the above dark matter core-collapse scenario to solve the problem of formation and growth of SMBHs at high z has led us to inquire further about it. Thus, we answer in this Letter three highly relevant questions left open in Argüelles et al. (2023b): (1) How does the dark matter core of fermions reach the point of gravitational collapse? (2) How long does it

take to the core to reach that point? (3) Are those conditions attainable in astrophysical and cosmological setups?

The answers to these questions arise from the fact that galaxy halos are not only made of dark matter but also have baryonic, i.e., ordinary matter. The baryonic matter infall into the potential well of the dark matter core modifies its equilibrium state. We calculate those new equilibrium configurations with the presence of baryonic matter and establish the existence of a critical mass for the gravitational collapse that depends upon the amount of baryonic matter settled in the core. The gravitational instability occurs because baryons contribute to the system energy density but not to the pressure, which is governed by the fermion degeneracy pressure in the dense dark matter core. We determine the threshold amount of baryonic mass and the minimum mass of the initial dark matter core leading to the SMBH formation (Section 2). We then show that SMBHs of $10^7 M_\odot$ can be formed from the baryon-induced collapse of dark matter cores in timescales shorter than 1 Gyr, for baryonic inner densities and velocities as obtained in cosmological simulations and observations (Section 3). Section 4 examines specific applications in galaxy mergers and the high-z Universe. By examining the data from the Chandra satellite and William Herschel Telescope of the Seyfert galaxy TXS 2116–077, we show that the merging timescale and jet lifetime agree with the SMBH originating from the baryon-induced collapse and that the inferred baryonic environment conditions for its occurrence agree with those observed. The baryon-induced collapse can also explain the formation of the $\sim 10^7$–$10^8 M_\odot$ farthest quasar, observed by the Chandra satellite at the center of the JWST-detected galaxy UHZ1 at $z = 10.3$. The same conclusions apply to the little red dots, the SMBHs at $z \approx 4$–6 also observed by JWST.

2. The Baryon-induced Collapse

The RAR model treats the dark matter in galaxies as a self-gravitating system of fermions at finite temperatures in equilibrium, so the general relativity field equations set the structure. The dark matter equation of state obeys Fermi–Dirac statistics and includes a particle energy cutoff, which determines the galaxy's finite size (see Argüelles et al. 2018; also Chavanis et al. 2015 for a Newtonian approach). The formation and stability of core–halo profiles with a Fermi–Dirac-like distribution function are predicted in structure formation scenarios of maximum entropy production principle (Chavanis 1998; Argüelles et al. 2021, 2023b). The equilibrium configuration is characterized by the segregation of the fermion physical regimes along the galaxy: a quantum degenerate core of nearly uniform density, followed by an intermediate semiclassical regime where the density falls off abruptly, followed by a plateau. Then, it follows a Boltzmann-like regime in the outer halo where the density falls off as a power law, followed by an exponential decrease determining the galaxy border. Figure 1 shows an example of a galactic dark matter profile for $m = 100 \text{ keV}/c^2$.

We focus hereafter on the equilibrium state of the core where fermions are in a degenerate regime. We can analyze the stability of this core by solving the Einstein equations for the simpler equation of state of a fermion gas at zero temperature. The energy density and pressure of such pure-dark-matter
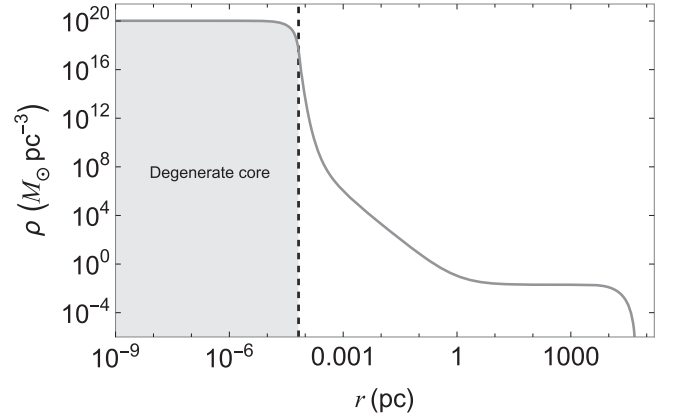

Figure 1. Pure-dark-matter equilibrium configuration with central density $\rho = 0.0068 \text{ g cm}^{-3} = 1.01 \times 10^{20} M_\odot \text{ pc}^{-3}$, for a fermion $m = 100 \text{ keV}/c^2$. The total halo mass is $5 \times 10^{11} M_\odot$. The degenerate quantum core (filled gray region) has a mass $M_{\rm dm} = 2.03 \times 10^7 M_\odot$ and radius $R_c = 6.67 \times 10^{-5}$ pc.

fermion gas are, respectively, $\mathcal{E} = \mathcal{E}_{\rm dm}$ and $P = P_{\rm dm}$, where

$$\mathcal{E}_{\rm dm} = \frac{mc^2}{8\pi^2\lambda^3}[\sqrt{1+x^2}\,(x+2x^3) - \text{arcsinh}(x)], \quad (1a)$$

$$P_{\rm dm} = \frac{mc^2}{24\pi^2\lambda^3}[x\sqrt{1+x^2}\,(2x^2-3) + \frac{3}{8}\text{arcsinh}(x)], \quad (1b)$$

with $\lambda = \hbar/(mc)$ as the particle Compton wavelength and $x = p_F/(mc)$ as the dimensionless Fermi momentum, which sets the particle rest-mass density, $\rho_{\rm dm} = m\, n_{\rm dm} = m\, x^3/(3\pi^2\lambda^3)$. The equilibrium configurations satisfy the Einstein equations in spherical symmetry for a perfect fluid, which can be written in the Tolman–Oppenheimer–Volkoff form (Oppenheimer & Volkoff 1939)

$$\frac{dM}{dr} = 4\pi r^2\rho, \quad \frac{dP}{dr} = -G\frac{(\rho + P/c^2)(4\pi r^3 P/c^2 + M)}{r(r - 2GM/c^2)}, \quad (2)$$

where M is the gravitational mass measured by an observer at rest at infinity. For instance, the solution of Equations (2) for a pure-dark-matter equilibrium configuration with central density $\rho = 6.8 \times 10^{-3} \text{ g cm}^{-3} \approx 10^{20} M_\odot \text{ pc}^{-3}$ leads to the density profile highlighted by the filled gray region in Figure 1, with mass $M_{\rm dm} = 2.03 \times 10^7 M_\odot$ and radius $R_c = 6.67 \times 10^{-5}$ pc.

Along a sequence of equilibrium configurations with increasing central density, the turning point, i.e., where $\partial M/\partial\rho_c = 0$, where $\rho_c = \mathcal{E}_c/c^2$, and the subscript c stands for values at the center ($r = 0$), sets the configuration of critical density and corresponding critical mass over which the core becomes unstable against gravitational collapse (Oppenheimer & Volkoff 1939). The critical mass of pure-dark-matter cores is (Argüelles et al. 2021, 2023b)

$$M_{\rm crit}^{(0)} \approx 0.38\frac{m_{\rm Pl}^3}{m^2} = 6.27 \times 10^7 \left(\frac{100 \text{ keV}/c^2}{m}\right)^2 M_\odot, \quad (3)$$

where $m_{\rm Pl} = \sqrt{\hbar c/G} = 2.18 \times 10^{-5}$ g is the Planck's mass. For $m = 100 \text{ keV}/c^2$ fermions, Equation (3) tells that the gravitational collapse of the dark matter core would lead to a BH mass $M_{\rm BH} = M_{\rm crit}^{(0)} = 6.27 \times 10^7 M_\odot$.

We are now interested in the modified equilibrium state of the core when it contains a composition of degenerate dark
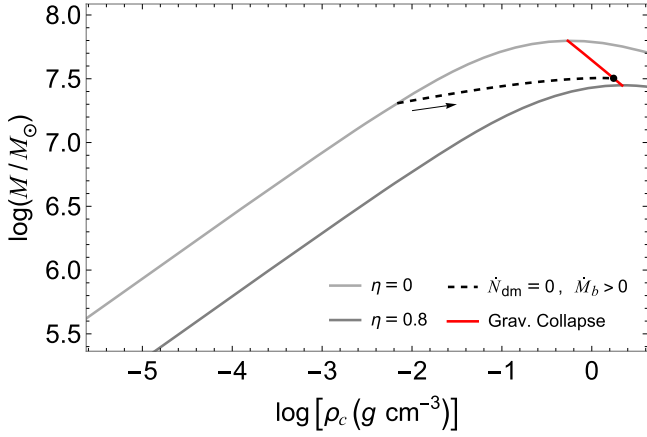
Figure 2. Dark matter+baryonic equilibrium configurations for $m = 100 \, \text{keV}/c^2$. The black dashed curve shows the equilibrium configurations at a constant total fermion number. The lighter and darker gray curves are the equilibrium sequences $\eta = 0$ and 0.8. The red curve is the secular instability limit for gravitational collapse. The black dashed sequence starts with a pure-dark-matter core ($\chi = 0$) of $M_{\text{dm}} = 2.03 \times 10^7 M_\odot$ and radius $R_c = 6.67 \times 10^{-5}$ pc, i.e., the degenerate core of the configuration shown in Figure 1. As baryons sink in the core, the configuration follows the black dashed sequence to the right (see the arrow) until it reaches the critical mass for gravitational collapse (black dot). The critical configuration has a baryon-to-dark-matter mass ratio $\chi_{\text{BH}} \approx 0.56$, so baryons contribute 36% and the dark matter 64% to the critical mass, $M_{\text{BH}} \approx 3.19 \times 10^7 M_\odot$, i.e., $M_{\text{dm,crit}} = 2.04 \times 10^7 M_\odot$ and $M_{b,\text{crit}} \approx 1.15 \times 10^7 M_\odot$.

matter fermions and ordinary/baryonic matter. For this task, we model the baryon content as dust, so the equation of state is now given by $\mathcal{E} = \mathcal{E}_{\text{dm}} + \mathcal{E}_b$, $P = P_{\text{dm}}$, where $\mathcal{E}_b = c^2 \rho_b$ is the energy density of baryons, where ρ_b is the baryon rest-mass density. The system of Equations (2) for this new equation of state can be integrated once we set a prescription to calculate ρ_b. We make the ansatz that the baryon rest-mass density follows the dark matter one, i.e., $\eta \equiv \rho_b/\rho_{\text{dm}} = $ constant. We construct the new equilibrium configuration sequences (M-ρ_c sequences) for different values of η. In Figure 2, we show the region of equilibrium configurations of dark matter+baryon cores for $0 \leqslant \eta \leqslant 0.8$, in the case of $m = 100 \, \text{keV}/c^2$. For every given ratio, the sequence turning point gives a critical mass configuration where $\partial M/\partial \rho_c = 0$. This procedure leads to the sequence of critical mass configurations given by the red curve in Figure 2. For the astrophysical analysis, using the baryon-to-dark-matter mass fraction $\chi = M_b/M_{\text{dm}}$ is more convenient. The pure-dark-matter core case ($\chi = 0$) is the first point (from top to bottom) of the critical configurations given by the red curve in the figure. The following analytical function fits the critical masses of the red curve:

$$M_{\text{BH}} \equiv M_{\text{crit}} \approx \frac{M_{\text{crit}}^{(0)}}{1 + 1.466 \chi_{\text{BH}} + 0.458 \chi_{\text{BH}}^2}, \quad (4)$$

where $\chi_{\text{BH}} \equiv \chi_{\text{crit}} = (M_b/M_{\text{dm}})_{\text{crit}} \approx M_{b,\text{crit}}/M_{\text{dm}}$, where $M_{b,\text{crit}}$ is the baryon mass at the point of critical mass, and $\dot{M}_{\text{dm}} \approx 0$ at 1% level along any constant-fermion-number track. The critical mass sets the SMBH mass formed from the collapse. It is worth emphasizing that Equation (4) is valid for any fermion mass m, for baryon-to-dark-matter mass ratios $0 \leqslant \chi_{\text{BH}} \lesssim 0.8$.

To exemplify the baryon-induced collapse, we show in Figure 2 a sequence of constant total dark matter particle number, N_{dm}, while the baryon number increases along the direction the arrow indicates. The sequence starts with a

pure-dark-matter core ($\chi = 0$) of gravitational mass $M_{\text{dm}} = 2.03 \times 10^7 M_\odot$, corresponding to a dark matter particle number $N_{\text{dm}} = 1.81 \times 10^{67}$. The core is surrounded by a diluted halo of $M_h \sim 10^{11} M_\odot$ as predicted by the RAR model (see Figure 1). According to Equation (3), the initial dark matter core is stable, i.e., $M_{\text{dm}} < M_{\text{crit}}^{(0)}$. However, the sequence intersects the instability sequence (red curve) at a critical mass of $M_{\text{BH}} = 3.19 \times 10^7 M_\odot$, for a critical baryon-to-dark-matter mass ratio $\chi_{\text{BH}} = 0.56$.

Therefore, the presence of baryons induces the collapse of an otherwise stable dark matter core, and the critical mass can be less than half of the critical mass of a pure-dark-matter core. But can dark matter cores gain those amounts of baryons in realistic astrophysical situations, at or about the moment of halo formation?

3. Baryon Gravitational Capture and Accretion Rate

To answer the above question, we analyze the astrophysical situation where the dark matter core captures baryons from an inner halo environment in the high-z Universe. The core capture baryons of rest-mass density $\bar{\rho}_b$ and speed v_b at a rate

$$\dot{M}_b = \pi R_{\text{cap}}^2 \bar{\rho}_b v_b, \quad (5)$$

where $R_{\text{cap}} = 2GM/v_b^2$ is the gravitational capture radius. It is worth emphasizing that $\bar{\rho}_b$ is the density of baryons at $r = R_{\text{cap}}$, which is expected to be much smaller than ρ_b inside the dark matter core. We solve the evolution equation $\dot{M} = \dot{M}_{\text{dm}} + \dot{M}_b$, which we can approximate to $\dot{M} \approx \dot{M}_b$ since we are assessing the evolution in a sequence $\dot{N}_{\text{dm}} = 0$ and $\dot{M}_{\text{dm}} \approx 0$ at the percent level. By integrating this equation, we obtain the mass and baryon-to-dark-matter mass ratio evolution

$$M(t) = \frac{M_{\text{dm}}}{1 - \bar{t}}, \quad \chi(t) = \frac{M_b(t)}{M_{\text{dm}}} = \frac{\bar{t}}{1 - \bar{t}}, \quad \bar{t} \equiv \frac{t}{\tau}, \quad (6)$$

$$\tau \equiv \frac{1}{4\pi G^2 Q_b M_{\text{dm}}} \approx \frac{421}{\bar{Q}_b} \left(\frac{10^7 M_\odot}{M_{\text{dm}}} \right) \text{Myr}, \quad (7)$$

where $Q_b = \bar{\rho}_b/v_b^3$ and $\bar{Q}_b \equiv Q_b/[(M_\odot/\text{pc}^3)/(100 \, \text{km s}^{-1})^3]$, and we recall that $M_{\text{dm}} = M(t = 0)$ is the initial mass that is that of the pure-dark-matter core. Equation (6) tells that the core reaches the critical mass for BH formation in a time

$$\bar{t}_{\text{BH}} = \frac{\chi_{\text{BH}}}{1 + \chi_{\text{BH}}} = 1 - \frac{M_{\text{dm}}}{M_{\text{BH}}}. \quad (8)$$

By replacing Equations (4) and (6) into Equation (8), we obtain an algebraic equation for χ_{BH} (or for $\bar{t}_{\text{BH}}$) that we solve with the aid of a Padé approximant and obtain

$$\chi_{\text{BH}} \approx -0.83 - \frac{0.09}{\mu} + \frac{\sqrt{0.008 + 0.896\mu - 0.054\mu^2}}{\mu}, \quad (9)$$

where $\mu \equiv M_{\text{dm}}/M_{\text{crit}}^{(0)}$, accurate at the 1% level.

Figure 3 shows t_{BH} for two selected examples, which, as we show in the next section, apply to two relevant astrophysical scenarios: the observed merging process of TXS 2116–077 with another nearby galaxy, and the farthest quasar recently observed by the Chandra X-ray satellite, located in the background galaxy UHZ1 at $z = 10.3$ observed by JWST. In these two typical examples, the dark matter core is given, correspondingly, by the
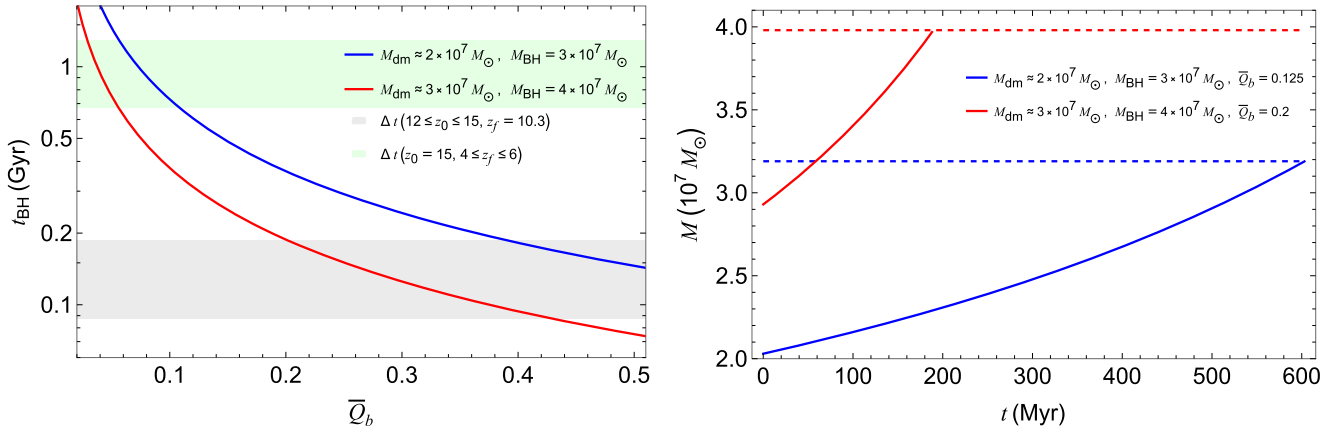
Figure 3. Left: time for SMBH formation by baryon-induced collapse as a function of $\bar{Q}_b$, for two selected examples of initial pure-dark-matter cores: $M_{\rm dm} = 2.03 \times 10^7 M_\odot$ (blue curve) and $M_{\rm dm} = 2.93 \times 10^7 M_\odot$ (red curve) that reach, respectively, the critical mass $M_{\rm BH} = 3.19 \times 10^7 M_\odot$ (dot in Figure 2) and $M_{\rm BH} = 3.98 \times 10^7 M_\odot$. The gray filled region shows the elapsed cosmological time from an initial redshift of $12 \leqslant z_0 \leqslant 15$ to a final redshift $z_f = 10.3$, relevant for the analysis of UHZ1*. Likewise, the green filled region from $z_0 = 15$ to $4 \leqslant z_0 \leqslant 6$ is relevant for analyzing the so-called little red dots. Right: time evolution of the dark matter core mass while accreting baryonic matter, given by Equation (6), for the two examples in the left panel, for the values of $\bar{Q}_b$ in the legend. The dashed lines indicate the SMBH mass formed. Details are given in Sections 3 and 4.

black dashed curve shown in Figure 2, which has an initial mass $M_{\rm dm} \approx 2 \times 10^7 M_\odot$ (blue curve in Figure 3), and by another core having $M_{\rm dm} \approx 3 \times 10^7 M_\odot$ (red curve in Figure 3). The time to BH formation is plotted as a function of $\bar{Q}_b$, for a range of astrophysically relevant values, e.g., as given by cosmological hydrodynamical simulations of the innermost gas density and velocity in high-z halos (Dekel & Birnboim 2006; Latif et al. 2022), as well as in giant molecular clouds and clumps in the Milky Way, local starbursts, and distant galaxies (see, e.g., Miville-Deschênes et al. 2017; Dessauges-Zavadsky et al. 2019, 2023). To exemplify, consider the initially stable core of $M_{\rm dm} = 2.03 \times 10^7 M_\odot$ (blue curve, accreting baryonic gas with $\bar{\rho}_b = M_\odot\,{\rm pc}^{-3}$ and $v_b = 200$ km s^{-1}; Dekel & Birnboim 2006), which leads to $\bar{Q}_b = 0.125$. The core attracts baryonic matter of such speed at $r = R_{\rm cap} = 4.36$ pc. From Equations (7)–(8), the baryon-induced collapse occurs at $t_{\rm BH} \approx 0.6$ Gyr, forming an SMBH of $3.19 \times 10^7 M_\odot$. Initially, the accretion rate is $\dot{M}_b = 0.012\,M_\odot$ yr^{-1}, leading to an accretion luminosity below the Eddington limit, i.e.,

$$L = \beta \dot{M}_b c^2 = \beta\,6.81 \times 10^{44}\ {\rm erg\ s}^{-1} < L_{\rm Edd}, \quad (10)$$

$$L_{\rm Edd} = \frac{4\pi G m_p c}{\sigma_T} M = 1.25 \times 10^{45} \left(\frac{M}{10^7 M_\odot}\right){\rm erg\ s}^{-1}, \quad (11)$$

where σ_T is the Thomson scattering cross section, m_p is the proton mass, and β is the efficiency in converting gravitational energy gain into electromagnetic radiation, which is below unity. The ratio $L/L_{\rm Edd}$ is proportional to M, so the maximum value attained by this ratio is obtained for $M_{\rm crit}/M_{\rm dm}$, which is of order unity (in the present example, 1.57). The accretion is sub-Eddington during the evolution to the critical mass point.

To be cautious, we have explored the occurrence of the baryon-induced collapse for different values of the baryon-to-dark-matter mass ratio, χ, limiting ourselves to a maximum of $\chi_{\rm max} \approx \eta_{\rm max} = 0.8$; see Figure 2. It is then clear from that figure that, given the maximum baryon-to-dark-matter mass ratio, there is a minimum constant-$N_{\rm dm}$ evolution (i.e., minimum $M_{\rm dm}$) below which no baryon-induced collapse occurs: the evolution track never crosses the red curve but a stable point of the $\eta_{\rm max} = 0.8$ sequence. Thus, we can estimate such a minimum mass of the initial pure-dark-matter core,

$M_{\rm dm}^{(min)}$, for the occurrence of the baryon-induced collapse. Again, that value is a function of the given $\chi_{\rm max}$. We can readily obtain $M_{\rm dm}^{(min)}$ by evaluating Equation (6) at the critical point for the maximum value of χ, i.e.,

$$M_{\rm dm}^{(min)} = \frac{M_{\rm BH}(\chi_{\rm max})}{1 + \chi_{\rm max}} \approx 0.22 M_{\rm crit}^{(0)}, \quad (12)$$

where, in the last expression, we have used Equation (4) with $\chi_{\rm max} \approx 0.8$. Therefore, for the fermion mass $m = 100$ kev/c^2, we obtain $M_{\rm dm}^{(min)} \approx 1.41 \times 10^7 M_\odot$.

Equation (12) tells us that independently of m, the maximum ratio $\chi_{\rm max}$ sets a minimum value of the ratio μ, i.e., $\mu_{\rm min} \equiv M_{\rm dm}^{(min)}/M_{\rm crit}^{(0)} \approx 0.22$. From Equation (9), it turns out that the maximum dimensionless BH formation time is set by $\mu = \mu_{\rm min}$, i.e., $\bar{t}_{\rm BH}^{\rm max} \equiv \bar{t}_{\rm BH}(\mu_{\rm min}) \approx 0.44$. Therefore, the maximum BH formation time is $t_{\rm BH}^{\rm max} = 0.44\,\tau_{\rm max}$, where $\tau_{\rm max}$ is the value of τ for $M_{\rm dm}^{(min)}$. By equating $t_{\rm BH}^{\rm max}$ to the universe lifetime (≈ 13.8 Gyr), we obtain an upper bound to m over which the present baryon-induced collapse mechanism can form no BH:

$$m_{\rm max} = 323.33 \sqrt{\frac{\bar{Q}_b}{0.1}}\ {\rm keV}/c^2. \quad (13)$$

Although the upper limit (13) depends on Q_b and has been obtained for the minimum pure-dark-matter core mass (which maximizes the BH formation time), it is remarkably similar to the upper bound of 350 keV/c^2 obtained from a different theoretical and observational request: that the dark matter halo explains the Milky Way rotation curves (Argüelles et al. 2018) and that the core explains the orbits of the S-cluster stars in alternative to the central BH scenario for Sgr A* (Becerra-Vergara et al. 2020, 2021).

4. Astrophysical Applications of the Baryon-induced Collapse

The SMBH formation by the baryon-induced collapse of dark matter fermion cores can trigger the activity at the center of galaxies by forming active galactic nuclei from merging events. This new scenario supports the hypothesis that relativistic jets in radio-loud active galactic nuclei are triggered

by galaxy mergers (see, e.g., Chiaberge et al. 2015). An interesting case is the Seyfert galaxy TXS 2116–077, which is merging with another nearby Seyfert galaxy on an estimated timescale of 0.5–2 Gyr. It hosts a radio jet with a kinematic age shorter than 15 kyr, considerably shorter than the merger timescale, strengthening the above hypothesis (Paliya et al. 2020). The derived mass of the central SMBH of TXS 2116–077 is $M_{\rm BH} \approx 3 \times 10^7 M_\odot$, which agrees with the example presented in Figure 2 (endpoint of the black dashed curve; blue curve in Figure 3). The initial dark matter core of $M_{\rm dm} \approx 2 \times 10^7 M_\odot$, accreting baryonic matter of density $\rho_b = 1\, M_\odot\, {\rm pc}^{-3}$ moving at 200 km s^{-1}, so $\bar{Q}_b = 0.125$, collapses forming such an SMBH in $t_{\rm BH} \approx 0.6$ Gyr; see Equations (7)–(8) and Figure 3. These baryonic matter conditions agree with the TXS 2116–077 inner region observations (Paliya et al. 2020), for a Compton thick active galactic nucleus with typical column density $N_H = 10^{24}$ cm^{-2}. The SMBH formation timescale increases (decreases) with decreasing (increasing) Q_b. It is worth recalling that the present theory predicts the core is surrounded by a dark matter halo of $M_h \sim 10^{11} M_\odot$ (see Figure 1), in agreement with the TXS 2116–077 total mass (Paliya et al. 2020).

Another case worth discussing is the farthest quasar ever detected, observed in the X-rays by the Chandra X-ray satellite, with a bolometric luminosity $L_{\rm bol} \approx 5 \times 10^{45}$ erg s^{-1} and associated SMBH mass $M_{\rm BH} \sim 10^7$–$10^8 M_\odot$, hosted by the JWST-detected lensed galaxy UHZ1 at $z \approx 10.3$ (Bogdán et al. 2023b). Assuming the SMBH accretes at the Eddington-limit rate, i.e., $L_{\rm bol} = L_{\rm Edd}$, we obtain from Equation (10), $M_{\rm BH} \approx 4 \times 10^7 M_\odot \approx 0.63 M_{\rm crit}^{(0)}$. Thus, from Equation (4), $\chi_{\rm BH} \approx 0.35$, which via Equation (8) leads to $\bar{t}_{\rm BH} \approx 0.26$, so the initial mass of the dark matter core is $M_{\rm dm} = 0.74\, M_{\rm BH} \approx 3 \times 10^7 M_\odot$. The red curve in Figure 3 shows this case, i.e., $t_{\rm BH} = 0.26\, \tau$, where τ is given by Equation (7). The gray filled region shows the cosmological time elapsed from an initial redshift $12 \leqslant z_0 \leqslant 15$ to the UHZ1 redshift, $z_f = 10.3$, which leads to 87.36 Myr $\lesssim t_{\rm BH} \lesssim$ 187.32 Myr. At fixed z_f, the larger the dark matter core seed redshift, z_0, the larger the time it has to accrete the necessary baryonic mass to trigger the collapse, so the smaller the Q_b. The cuts of the gray filled region with the red curve give this example's corresponding range of solutions, i.e., $0.20 \lesssim \bar{Q}_b \lesssim 0.43$. This range suggests ρ_b in UHZ1 about twice that of TXS 2116–077 (for similar v_b), in line with the column densities of Bogdán et al. (2023b).

An SMBH of a larger mass than the above value would imply that the dark matter core collapsed at $z > 10.3$ and then continued to accrete until reaching that mass at $z_f = 10.3$. Let us assume the SMBH has the largest inferred value from the observations, $M_{\rm BH}(z_f = 10.3) = 10^8 M_\odot$. The dark matter core collapsed at $z_c > z_f$, forming an SMBH of mass $M_{\rm BH}(z_c) = 4 \times 10^7 M_\odot$. Thus, from z_c to z_f, the newborn SMBH accreted $6 \times 10^7 M_\odot$. The SMBH mass $M_{\rm BH}(z_f)$ implies $L_{\rm bol}/L_{\rm Edd} = 0.4$. Assuming this ratio holds constant at this value, the time it takes for the BH to increase its mass from $M_{\rm BH}(z_c)$ to $M_{\rm BH}(z_f)$ is $\Delta t = 59.26$ Myr, for a gravitational-to-electromagnetic energy conversion factor $\beta = 0.057$, set by the binding energy of the last stable circular orbit for a Schwarzschild BH. Thus, the dark matter core collapsed at $z_c \approx 11.39$. If the dark matter core–halo distribution formed, e.g., at $z_0 = 15$, the baryon-induced collapse of the dark matter core must occur in $t_{\rm BH} = 127.88$ Myr, achievable for $\bar{Q}_b \approx 0.29$ (see Figure 3).

Therefore, the baryon-induced collapse of fermion dark matter cores explains the formation of SMBHs at high z. Consequently, it can also explain the little red dots, i.e., the SMBHs of 10^7–$10^8 M_\odot$ at $z \approx 4$–6 observed by JWST (see, e.g., Kocevski et al. 2023; Matthee et al. 2023), for $\bar{Q}_b \sim 0.1$ (see Figure 3). Interestingly, the mean value of the little red dots' bolometric luminosity is $L_{\rm bol}/L_{\rm Edd} \approx 0.2$, similar to our previous example. Future studies can infer the SMBH mass function of the baryon-induced collapse scenario and compare it with the observed SMBH population at various redshifts.

5. Conclusions

How SMBHs form and grow at high cosmological redshifts has remained elusive for years (Volonteri 2012; Woods et al. 2019). The relevance of getting a satisfactory answer is exponentially increasing with the advent of JWST's new, deep observations of the Universe spacetime unveiling the farthest quasars ever detected (Yang et al. 2021; Gilli et al. 2022; Fan et al. 2023; Kocevski et al. 2023; Maiolino et al. 2023; Yue et al. 2023).

In Argüelles et al. (2023b), it was shown that the collapse of dark matter cores made of 50–100 keV/c^2 fermions would lead to heavy BH seeds of 10^7–$10^8 M_\odot$, which could grow further by sub-Eddington accretion of baryonic matter to reach $10^9 M_\odot$ in comfortable timescales of the order of 1 Gyr or less. This Letter answered the crucial questions of how a dark matter core reaches gravitational collapse conditions, how long that process could take, and how those conditions are realized in astrophysics and cosmology.

We have shown that an initially stable dark matter core, with a mass larger or equal to 22% of the critical mass of a pure-dark-matter core, i.e., without ordinary/baryonic matter, can reach a point of gravitational collapse by gaining some threshold amount of baryons. We calculate such a critical mass for SMBH formation as a function of the baryon-to-dark-matter mass ratio. We limited our analysis to a maximum ratio of $\sim$80%. For this maximum ratio, the dark matter+baryon core critical mass is $\sim$40% lower than that of a pure-dark-matter core. For $m = 100$ keV/c^2 fermions, this baryon-induced collapse process leads to an SMBH of $\sim 10^7 M_\odot$. We provided analytical formulas for the SMBH mass as a function of the baryon-to-dark-matter mass ratio and the minimum mass of the initial dark matter core for the baryon-induced collapse to occur.

The gravitational capture of baryons from the environment triggers the gravitational collapse when it accumulates a threshold amount of baryons that instabilizes the core equilibrium. The needed accretion rate is sub-Eddington for baryonic densities ($\rho_b \sim M_\odot$ pc^{-3}) and velocities ($v_b \sim 100$ km s^{-1}) leading to $Q_b = \rho_b / v_b^3$ values typical in cosmological hydrodynamical simulations of high-z halos (Dekel & Birnboim 2006; see also Latif et al. 2022) and observations of giant molecular clouds and clumps in the Milky Way, local starbursts, and distant galaxies (Miville-Deschênes et al. 2017; Dessauges-Zavadsky et al. 2019, 2023). The above process forms $\sim 10^7 M_\odot$ SMBHs in timescales shorter than 1 Gyr, for $m = 100$ keV/c^2 fermions.

The SMBH formation timescale increases with the square of the fermion mass, so we obtain an upper bound to the latter of $m_{\rm max} \approx 323$ keV/c^2 for the collapse to occur in timescales shorter than the Universe age, for a typical value of Q_b. The upper limit depends on Q_b as $m_{\rm max} \propto \sqrt{Q_b}$. Imposing shorter timescales for the SMBH formation leads to a more stringent value of the dark matter fermion mass upper bound (at fixed Q_b).

Therefore, the accretion of baryonic matter by dark matter cores in the high-z Universe can lead to SMBHs by baryon-induced collapse in a fraction of 1 Gyr, which can further grow up to $\sim 10^8$–$10^9 M_\odot$ as required by the observations of the farthest quasars (Argüelles et al. 2023b). We have shown the viability of the baryon-induced collapse mechanism in three relevant cases: the formation of the SMBH in the Seyfert galaxy TXS 2116–077 in the merger with a nearby galaxy; the farthest quasar ever observed, located at $z = 10.3$ at the center of the galaxy UHZ1; and the little red dots at $z \approx 4$–6.

The assessment of the above results of SMBH formation, together with the complementary application of the RAR model on galactic dynamics and structure formation (see, e.g., Argüelles et al. 2023a), point to a neutral, massive, spin $1/2$ fermion with rest mass-energy between the one of active neutrinos and the one of electrons, of about 100 keV. Does this fermion fit with any known dark matter particle candidates? A natural dark matter candidate that could be associated with our fermion is the right-handed sterile neutrinos introduced in the minimum standard model extension, νMSM (Shaposhni-kov 2008). Under this assumption, we studied an extension of the RAR model with fermion self-interactions via a dark-sector massive (axial) vector mediator (Argüelles et al. 2016) and calculated the self-interaction cross section via an electroweak-like treatment. The latter was constrained using the bullet cluster and X-ray NuSTAR data from the Milky Way's central parsec, assuming the sterile neutrinos decay channel into photons (X-rays) and light (active) neutrinos. This analysis allows a ~ 100 keV fermion mass (Yunis et al. 2020). On the other hand, promising direct searches of dark matter in terrestrial laboratories, e.g., xenon, krypton, and argon detectors, via the dark matter interactions with ordinary matter, electrons, and nucleons, via kinetic energy recoils or even target ionization have started to look for a dark matter fermion in the tens of keV range (see, e.g., Dror et al. 2020; Shakeri et al. 2020; Dror et al. 2021; Aprile et al. 2022; Ge et al. 2022; Li et al. 2022; Zhang et al. 2022; Aalbers et al. 2023; Abe et al. 2023; Caddell et al. 2023; PandaX Collaboration et al. 2023; Rebeiro et al. 2023; Smirnov & Trautner 2023, and references therein). This is precisely the fermion mass-energy range that we have inferred from combined astrophysical analyses.

The baryon-induced collapse of dark matter fermion cores, by answering the long-standing question of how SMBHs form and grow in the high-z Universe, adds a piece to the possible role of a yet-unobserved massive fermion in the Universe. It opens a research window verifiable especially with the JWST and Euclid data, to further constrain the fermionic dark matter hypothesis. These constraints, combined with information from galactic dynamics, strengthen the synergy between astrophysics and terrestrial laboratories of direct searches of a light dark matter particle below MeV energies.

ORCID iDs

C. R. Argüelles ⓘ https://orcid.org/0000-0002-5862-8840
J. A. Rueda ⓘ https://orcid.org/0000-0003-4904-0014
R. Ruffini ⓘ https://orcid.org/0000-0003-0829-8318

References

Aalbers, J., AbdusSalam, S. S., Abe, K., et al. 2023, JPhG, 50, 013001
Abe, K., Hayato, Y., Hiraide, K., et al. 2023, PhRvL, 130, 031802
Aprile, E., Abe, K., Agostini, F., et al. 2022, PhRvL, 129, 161805
Argüelles, C. R., Becerra-Vergara, E. A., Rueda, J. A., & Ruffini, R. 2023a, Univ, 9, 197
Argüelles, C. R., Boshkayev, K., Krut, A., et al. 2023b, MNRAS, 523, 2209
Argüelles, C. R., Díaz, M. I., Krut, A., & Yunis, R. 2021, MNRAS, 502, 4227
Argüelles, C. R., Krut, A., Rueda, J. A., & Ruffini, R. 2018, PDU, 21, 82
Argüelles, C. R., Krut, A., Rueda, J. A., & Ruffini, R. 2019, PDU, 24, 100278
Argüelles, C. R., Mavromatos, N. E., Rueda, J. A., & Ruffini, R. 2016, JCAP, 1604, 038
Argüelles, C. R., Mestre, M. F., Becerra-Vergara, E. A., et al. 2022, MNRAS, 511, L35
Arita, J., Kashikawa, N., Matsuoka, Y., et al. 2023, ApJ, 954, 210
Becerra-Vergara, E. A., Argüelles, C. R., et al. 2020, A&A, 641, A34
Becerra-Vergara, E. A., Argüelles, C. R., Krut, A., Rueda, J. A., & Ruffini, R. 2021, MNRAS, 505, L64
Begelman, M. C., Rossi, E. M., & Armitage, P. J. 2008, MNRAS, 387, 1649
Begelman, M. C., Volonteri, M., & Rees, M. J. 2006, MNRAS, 370, 289
Bogdan, A., Goulding, A., Natarajan, P., et al. 2023a, NatAs, Advanced Online Publication
Bogdán, Á., Goulding, A. D., Natarajan, P., et al. 2023b, NatAs, Advanced Online Publication
Caddell, A. R., Flambaum, V. V., & Roberts, B. M. 2023, PhRvD, 108, 083030
Chavanis, P.-H. 1998, MNRAS, 300, 981
Chavanis, P.-H., Lemou, M., & Méhats, F. 2015, PhRvD, 92, 123527
Chiaberge, M., Gilli, R., Lotz, J. M., & Norman, C. 2015, ApJ, 806, 147
Dekel, A., & Birnboim, Y. 2006, MNRAS, 368, 2
Dessauges-Zavadsky, M., Richard, J., Combes, F., et al. 2019, NatAs, 3, 1115
Dessauges-Zavadsky, M., Richard, J., Combes, F., et al. 2023, MNRAS, 519, 6222
Dror, J. A., Elor, G., McGehee, R., & Yu, T.-T. 2021, PhRvD, 103, 035001
Dror, J. A., Elor, G., & McGehee, R. 2020, PhRvL, 124, 181301
Fan, X., Bañados, E., & Simcoe, R. A. 2023, ARA&A, 61, 373
Ge, S.-F., He, X.-G., Ma, X.-D., & Sheng, J. 2022, JHEP, 2022, 191
Gilli, R., Norman, C., Calura, F., et al. 2022, A&A, 666, A17
Hosokawa, T., Hirano, S., Kuiper, R., et al. 2016, ApJ, 824, 119
Inayoshi, K., Visbal, E., & Haiman, Z. 2020, ARA&A, 58, 27
Kocevski, D. D., Onoue, M., Inayoshi, K., et al. 2023, ApJL, 954, L4
Krut, A., Argüelles, C. R., Chavanis, P. H., Rueda, J. A., & Ruffini, R. 2023, ApJ, 945, 1
Larson, R. L., Finkelstein, S. L., Kocevski, D. D., et al. 2023, ApJL, 953, L29
Latif, M. A., Whalen, D. J., Khochfar, S., Herrington, N. P., & Woods, T. E. 2022, Natur, 607, 48
Li, T., Liao, J., & Zhang, R.-J. 2022, JHEP, 2022, 71
Madau, P., & Rees, M. J. 2001, ApJL, 551, L27
Maiolino, R., Scholtz, J., Curtis-Lake, E., et al. 2023, arXiv:2308.01230
Matthee, J., Naidu, R. P., Brammer, G., et al. 2023, arXiv:2306.05448
Miville-Deschênes, M.-A., Murray, N., & Lee, E. J. 2017, ApJ, 834, 57
Oppenheimer, J. R., & Volkoff, G. M. 1939, PhRv, 55, 374
Pacucci, F., Nguyen, B., Carniani, S., Maiolino, R., & Fan, X. 2023, ApJ, 957, L3
Paliya, V. S., Pérez, E., García-Benito, R., et al. 2020, ApJ, 892, 133
PandaX Collaboration, Ning, X., Abdukerim, A., et al. 2023, Natur, 618, 47
Rebeiro, B. M., Triambak, S., Garrett, P. E., et al. 2023, PhRvL, 131, 052501
Ruffini, R., Argüelles, C. R., & Rueda, J. A. 2015, MNRAS, 451, 622
Shakeri, S., Hajkarim, F., & Xue, S.-S. 2020, JHEP, 2020, 194
Shaposhnikov, M. 2008, JHEP, 08, 008
Smirnov, A. Y., & Trautner, A. 2023, PhRvL, 131, 021002
Volonteri, M. 2012, Sci, 337, 544
Volonteri, M., Habouzit, M., & Colpi, M. 2021, NatRP, 3, 732
Woods, T. E., Agarwal, B., Bromm, V., et al. 2019, PASA, 36, e027
Woods, T. E., Heger, A., Whalen, D. J., Haemmerlé, L., & Klessen, R. S. 2017, ApJL, 842, L6
Yang, J., Wang, F., Fan, X., et al. 2021, ApJ, 923, 262
Yue, M., Eilers, A.-C., Simcoe, R. A., et al. 2023, arXiv:2309.04614
Yunis, R., Argüelles, C. R., Mavromatos, N. E., et al. 2020, PDU, 30, 100699
Zhang, D., Abdukerim, A., Bo, Z., et al. 2022, PhRvL, 129, 161804
Zhu, Q., Li, Y., Li, Y., et al. 2022, MNRAS, 514, 5583